Maximizing particle concentration in deterministic lateral displacement arrays

Shilun L. Feng,[1,4] Alison M. Skelley,[2] Ayad G. Anwer,[3,4] Guozhen Liu,[3,4] and David W. Inglis[1,4]
[1]*Department of Engineering, Macquarie University, Sydney, NSW 2109, Australia*
[2]*GPB Scientific LLC, 800 East Leigh St., Richmond, Virginia 23219, USA*
[3]*Department of Physics and Astronomy, Macquarie University, Sydney, NSW 2109, Australia*
[4]*ARC Centre of Excellence for Nanoscale BioPhotonics, Macquarie University, Sydney, NSW 2109, Australia*

(Received 16 January 2017; accepted 4 April 2017; published online 28 April 2017)

We present an improvement to deterministic lateral displacement arrays, which allows higher particle concentration enhancement. We correct and extend previous equations to a mirror-symmetric boundary. This approach allows particles to be concentrated into a central channel, no wider than the surrounding gaps, thereby maximizing the particle enrichment. The resulting flow patterns were, for the first time, experimentally measured. The performance of the device with hard micro-spheres and cells was investigated. The observed flow patterns show important differences from our model and from an ideal pattern. The 18 μm gap device showed 11-fold enrichment of 7 μm particles and nearly perfect enrichment—of more than 50-fold—for 10 μm particles and Jurkat cells. This work shows a clear path to achieve higher-than-ever particle concentration enhancement in a deterministic microfluidic separation system. *Published by AIP Publishing*. [http://dx.doi.org/10.1063/1.4981014]

I. INTRODUCTION

Microfluidic science and engineering has provided a number of novel and useful improvements over conventional laboratory techniques in the field of cell and particle enrichment and separation. Conventional methods such as membrane filtration utilize a filter with a range of pore sizes and result in a poor sized-based discrimination especially for differentiating between cell sizes. Track-etched filter membranes offer much improved control of pore size, but these retain cells and particles above the filter cutoff size on the membrane, and thus foul quickly for larger volume or higher cell/particle concentrations. The microfluidic solution is to create flow-through systems that, instead of trapping the larger particles, isolate these particles into a different moving stream, hence providing one stream containing all the cells, particles, and soluble molecules below the cutoff size and one containing all the cells/particles above that size.

The microfluidic approaches operate over a range of flow rates and Reynolds numbers and are differentiated by how the size discrimination is made. Methods such as deterministic lateral displacement (DLD)[1–3] and branch flow filtration (BFF)[4] use carefully designed features such as posts or branching channels to capture the particle-free boundary layer that exists against all surfaces. Other microfluidic approaches operate at moderate to higher Reynolds numbers where size-dependent inertial forces alter the trajectories of particles.[5] As the sample travels through the channels at high flow rates, the cells and particles of different sizes are shifted to different locations in the fluid stream. The utility of inertial separations is enhanced by combining it with secondary recirculating Dean flows in curved channels.[6]

While the majority of the literature focuses on separation, enrichment is fundamentally linked to separation and the devices discussed above can serve dual purposes. Branch flow filtration (BFF) has the potential to achieve high enrichment through the use of a great many branches each taking a small amount of fluid from a larger input channel.[8] Shevkoplyas *et al*. have recently shown two promising devices with a theoretical enrichment of 24 and demonstrated an

enrichment of 15,[9,10] respectively. However, in a continuous-flow microfluidic process, enrichment of the desired product is challenging in part because the increasing particle or cell concentration may affect the local fluid properties and prevent proper function of the device, thus limiting the practical operational limits.

In BFF, particles above the size cut-off can be pushed into a branch channel and permanently contaminate the filtered product. In contrast, devices that use inertial separations or DLD can overcome particle-particle interactions by using longer devices that provide additional redundancy, giving particles that occasionally fail to be separated more chances. DLD has shown good performance at high volume fractions, including whole blood.[11]

Recent work on inertial separations by Warkiani[7] has also shown excellent progress at working with high volume fractions (up to 10^7 cells per ml), but the device produces only 2× enrichment per pass. Inertial separations focus the desired particles to a position that is far (a few particle diameters) away from any surface. Capturing the desired particles in a 2D chip thus requires capturing a large volume of the surrounding fluids. This excess volume limits the enrichment factor.

Conversely, concentrating or enriching particles using DLD is typically done by laterally displacing them toward a wall where they continue to flow but increase in concentration. Huang *et al*. demonstrated over 100× enrichment of 61 and 158 kb DNA fragments in an electrophoretically driven device with 1.5 μm gaps.[1] The boundaries in this work (Figure 4(C) of Ref. 1) are not described but appear to be carefully tailored. Previous work by Inglis[12] described modifications to the boundaries, but the approximations used to derive flux through the gaps were not correct. Here, we describe a general approach to boundary modification in DLD arrays with a mirror symmetric particle accumulation boundary or central channel. We present a device with two mirror-symmetric arrays on either side of a common central channel that represents a 2× improvement in the possible particle enrichment over prior DLD art, resulting in a net 50 fold enrichment of 10 μm particles and Jurkat cells.

II. THEORY

We consider a device with a single input, a product output, and a waste output. The device has a line of symmetry in the middle causing particles that are larger than a critical size to move toward this central axis of symmetry. The critical size is a function of the slope (θ) or row shift fraction epsilon (ε), where $\varepsilon = \tan\theta$ and ε is 1 over an integer N. We follow the same approach as Huang *et al*.[1] and divide the fluid flux through each gap into N streamlines, where streamlines are delineated by stall lines emanating from stagnation points on obstacles in subsequent rows of the array. The width of the first streamline in each gap is represented by the symbol β and is defined as the minimum horizontal distance to the obstacle surface and the adjacent stall line that terminates on the next row of posts downstream (Fig. 1). We assume that the width of the first streamline is approximately equal to the radius of the largest particles that can follow the fluid flow direction. We define ideal bumping as particles with radii that are larger than the width of the first streamline being laterally displaced by the row shift at every row.

Consider an array that is intended to concentrate particles and is W gaps wide. After N rows, large particles will be laterally shifted by 1 column. Under ideal conditions, the length of the array must be at least W/ε (or W*N) rows long to allow all particles to migrate across the array. If the array is mirrored so that particles bump to the centre, the minimum length is W/(2ε). The array is typically made about 40% longer than this to ensure complete concentration in non-ideal circumstances. At the end of the device, all particles above the critical size are flowing in the centre channel causing a W fold increase in the number-density of particles.

Achieving this concentration enhancement requires particles be laterally displaced effectively in all regions of the array, including the central channel where particles accumulate. The flow patterns around the central channel can be modified by tailoring the shape and position of posts at the boundary, without introducing features that are smaller than in the bulk of the array. Previous work[12] described modifications to the lateral boundaries of a DLD array that

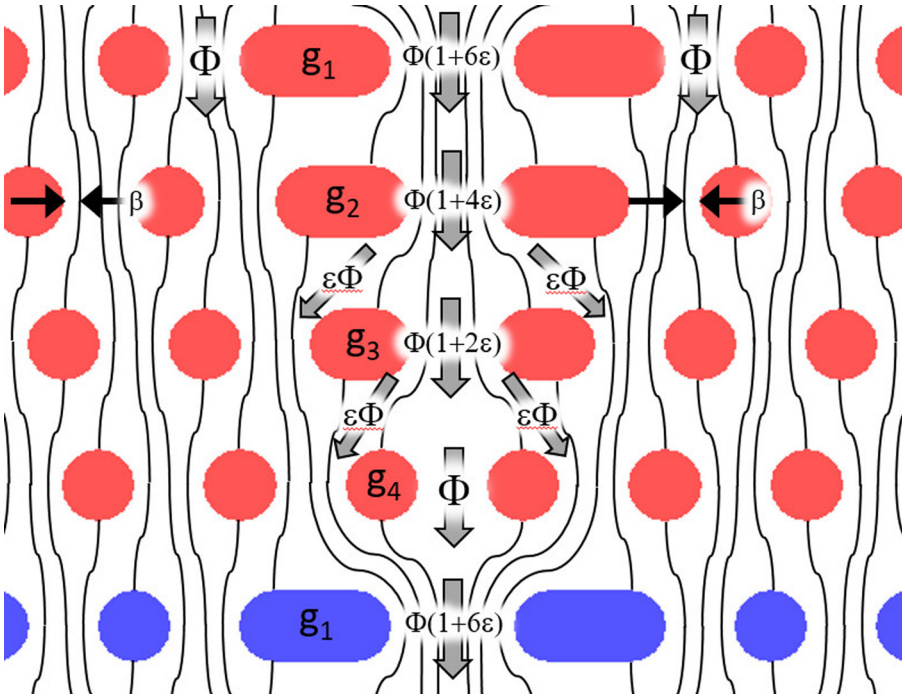

FIG. 1. Schematic highlighting streamlines in an ideal DLD array with $\varepsilon = 1/4$. Each gap in the main array carries a flux of Φ. Particles are bumped into the central channel between g4 and g1 and then remain in the central channel as small amounts of fluid leave to the left and right. This maintains the essential fluid flow pattern in all regions of the array.

drastically improved bumping near those boundaries. The author assumed that the flux through a gap is proportional to the square of the gap width. For a very deep and narrow gap with a large pillar diameter, we can approximate the geometry as parallel plates and solve the 2D Stokes equation exactly for the plane Poiseuille flow result. The flux through such a gap is

$$\Phi = \frac{2d}{3\mu}\Delta P g^3, \tag{1}$$

where d is the channel depth, μ is the viscosity, ΔP is the pressure gradient, and g is the gap width. The flux is therefore proportional to the cube of the gap instead of the square value used previously.

In this work, our fabrication process limits the depth to about twice the gap width and the plane Poiseuille approximation no longer applies. Supplementary material Figure 1 plots the flux through a rectangular channel versus channel width. For a depth of 40 μm and a width of between 18 and 30 μm, it is reasonable to assume that flux is proportional to gap squared.

Figure 1 shows an array with a row shift fraction of $^1/_4$. It shows exactly how much fluid should pass through each gap for there to be a consistent critical size at all gaps. The amount of fluid flux that transitions from one gap over the top of a post to an adjacent gap is $\varepsilon\Phi$. At $g = 1$, the flux in the centre gap is $\Phi\ (1 + (N-1)\varepsilon)$; at each row, the centre gap loses $2\varepsilon\Phi$. At g_N, the gap is the same as in the bulk array and the flux is Φ. If we normalise the flux through a gap (G) in the bulk array so that $\Phi = 1$, then the flux through any gap is $(g/G)^2$, where g is the width of the modified gap. The task is to modify the gaps in the central channel, so that they pass the intended amount of fluid flux.

This pattern of flux in the central gap leads to the following expression for the gap in the centre channel:

$$g_n = G\sqrt{3 - 2n\varepsilon} \quad \text{for } 0 \le n \le N. \tag{2}$$

Note that for gaps that are much smaller than the channel depth, the square root should be replaced with a cube root. In some cases, such as a cascaded DLD chip with a decreasing gap size, it is necessary to use a central gap that is larger than the adjacent array gap. It is possible to extend this approach for this need. For example, if the central gap should never be smaller than 1.5 G, this central gap must always carry an additional $(1.5^2 - 1) = 1.25$ units of flux. Equation (2) becomes $g_n = G\sqrt{1.25 + 3 - 2n\varepsilon}$.

III. RESULTS

A. Streamline tracing

To test our derivation of the flux in the central gap, a device with 18 μm gaps (in the bulk array), 18 μm diameter pillars, and a row shift fraction (ε) of 1/30 was fabricated with a depth of 40 μm as described in Section VI. The total array length is 40.0 mm (29.1 mm is needed under ideal bumping conditions). Gaps in the centre channel are given by Equation (2) and range from 18 to 30.8 μm. Figure 2 shows the entire device layout. We observed fluid streamlines in the chip by slowly flowing 0.5 μm fluorescent microspheres and recording their paths.

Figure 3(b) shows an example image used to measure streamline widths. The red curves follow an inferred stall line that terminates at the stagnation point on the large post adjacent to g_1. As the curve passes through the gap, the distance from this line to the nearest post is measured and plotted with open circles in Figure 3(a). The error bars represent the measurement uncertainty.

The streamline width at g_{30} has an average width of 4.0 μm. This means that particles with diameters up to 8 μm will flow to the outside of the large post g_1 and not be concentrated into the central channel. This matches our observations described in Section III B.

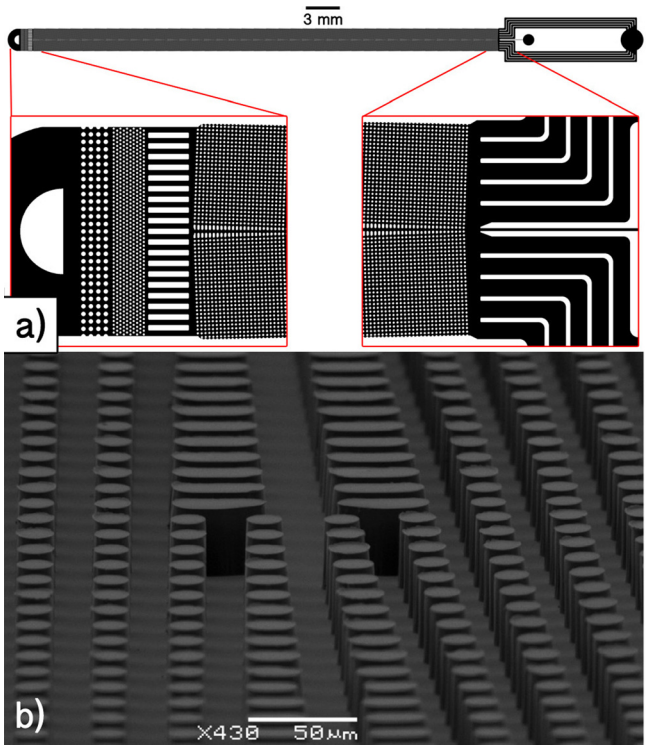

FIG. 2. (a) Full device layout with blow-ups of the inlet (left) and outlet regions (right). (b) SEM image of the centre channel of the PDMS device.

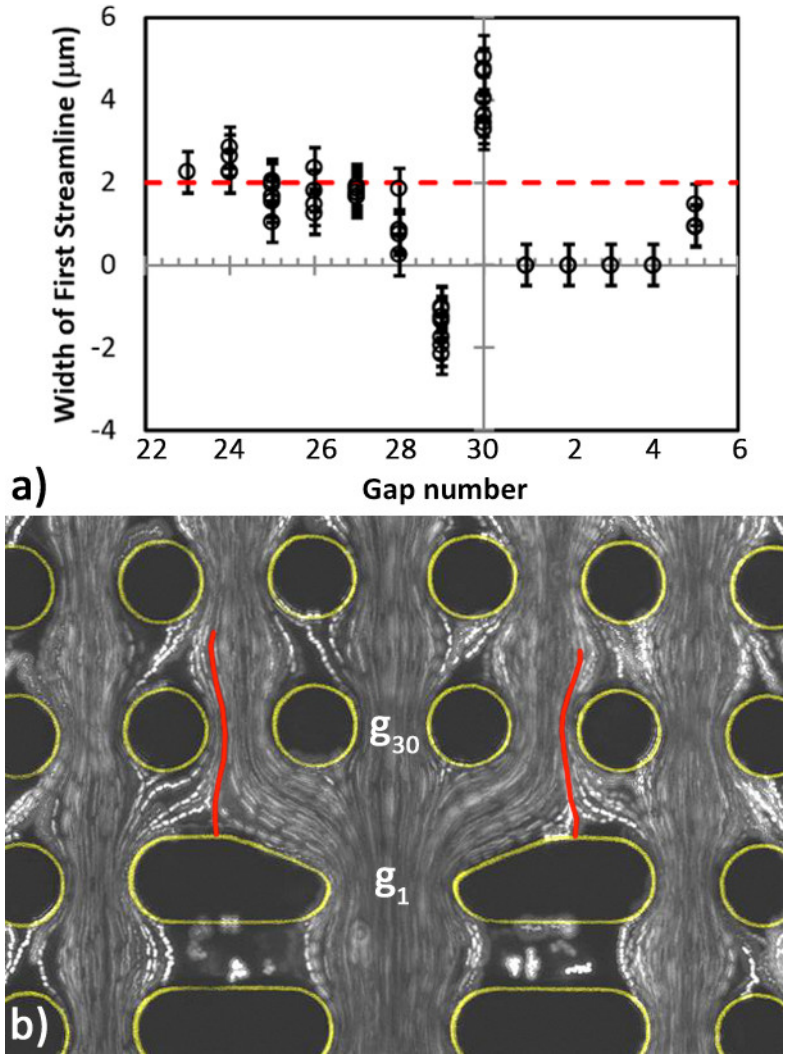

FIG. 3. (a) Experimentally measured first streamline width. This is conventionally assumed to be equal to the critical radius. An ideal plot would be flat at 2.0 μm (dashed red line). (b) Example image used to measure streamline width. The horizontal distance between the red line and the post edge is the streamline width at gap number 30.

B. Bead enrichment

The predictions based on streamline tracing are supported by experiments with beads ranging from 5 to 10 μm. Beads with 5 and 6 μm diameter showed little concentration enrichment, Beads with the size of 7.3 μm are bumped away from the negative edges but showed only slight enrichment in the central gap (21%) (Fig. 4(c)). Beads with the size of 7.3 μm bumped correctly in most regions but generally executed a zig-zag pattern and failed to move into the central channel between g_{30} and g_1 (Fig. 4(a)). Enrichment is defined as the fraction of cells in the centre gap times the width of the device in gaps (The device is 54 gaps wide). At the end of the array (shown in Figure 4(b)), the concentration enhancement for 7.3 μm beads is $54 \times 0.21 = 11$-fold. Beads with the size of 9.9 μm bump very well in all regions of the chip and resulted in 95% of beads exiting the array in the centre gap for a concentration enhancement of $54 \times 0.95 = 51$-fold.

C. Cell enrichment

Jurkat cells with an average diameter of 8.9 ± 1.4 μm ($N = 20$) showed superb enrichment or concentration enhancement in the device across all pressures tested at densities of 10^6 cells/ml.

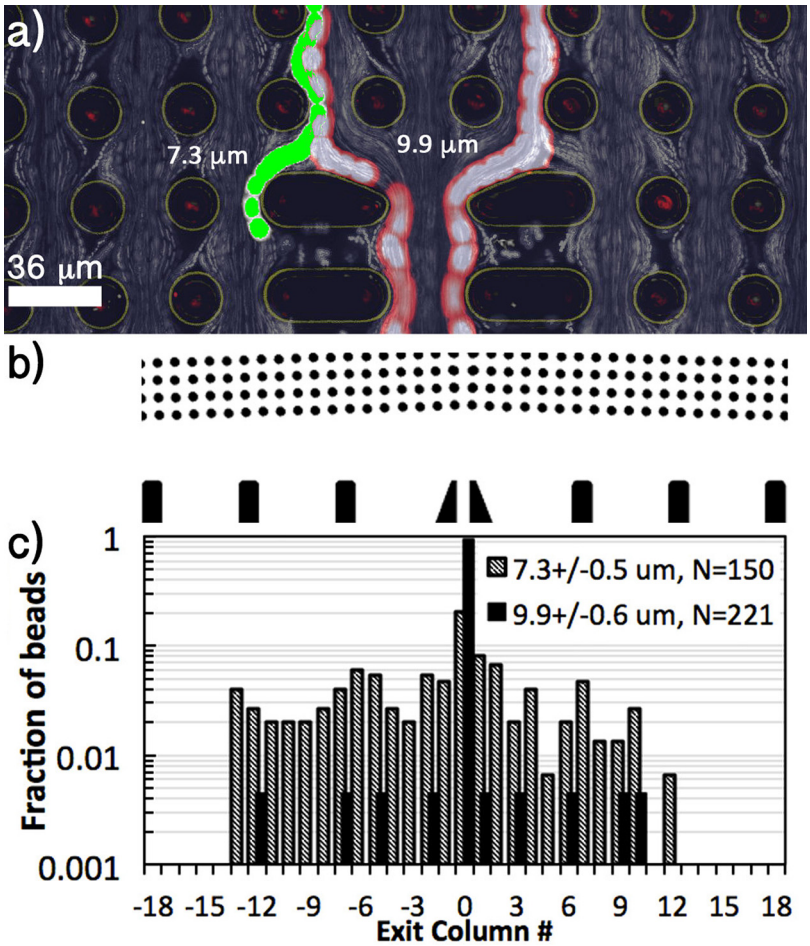

FIG. 4. Performance of microbead concentration. Flow is top to bottom: (a) overlay of post geometry (yellow); 0.5 μm bead paths (white), and example 9.9 μm (red) and 7.3 μm (green) bead(s); (b) layout at the end of the DLD array. The centre gap is the exit column #0, and each gap is numbered; (c) normalized histograms of the exit position for 7.3 and 9.9 μm beads. Beads with the size of 7.3 μm show 21% in the central gap, and 10 μm beads show 95% in central gap.

Figure 5(a) shows a single cell bumping through the end of one section and into the subsequent section. Figure 5(b) shows an ensemble of fluorescently labelled cells moving in the displacement mode (bumping) towards the centre channel. Figure 5(c) shows the percentage of cells flowing in the centre gap at the end of the array. More than 99% capture efficiency was observed across more than 2000 cells at pressures up to 500 mbar.

The flow rate through the chip is 110 μl/min at 500 mbar (0.5 atm). The gaps are 18 μm wide and 40 μm tall so an assumption of a parabolic flow profile in the gaps is reasonable for the purpose of estimating shear. The maximum shear rate in a parabolic flow is $4U_{max}/G$, where U_{max} is the maximum velocity and G is the gap width. The average velocity U_{ave} is $2/3U_{max}$. The total flow rate of 110 μl/min (1.83 mm^3/s) equals $54GdU_{ave}$, where d is the device depth of 40 μm. This gives in each gap a U_{ave} of 47 mm/s and a peak shear of 15 700 s^{-1}. At this speed, the Reynolds number is about 0.8.

IV. DISCUSSION

The performance of the chip for 10 μm beads and cells is excellent; however, there is room for improvement in the performance of 5–8 μm particles. A bulk array with our dimensions (gap of 18 and $\varepsilon = 1/30$) is expected to have a first streamline width of 2.0 μm (Ref. 2) and a critical size of 4.9 μm (Ref. 3), with the array concentrating all particles larger than this by

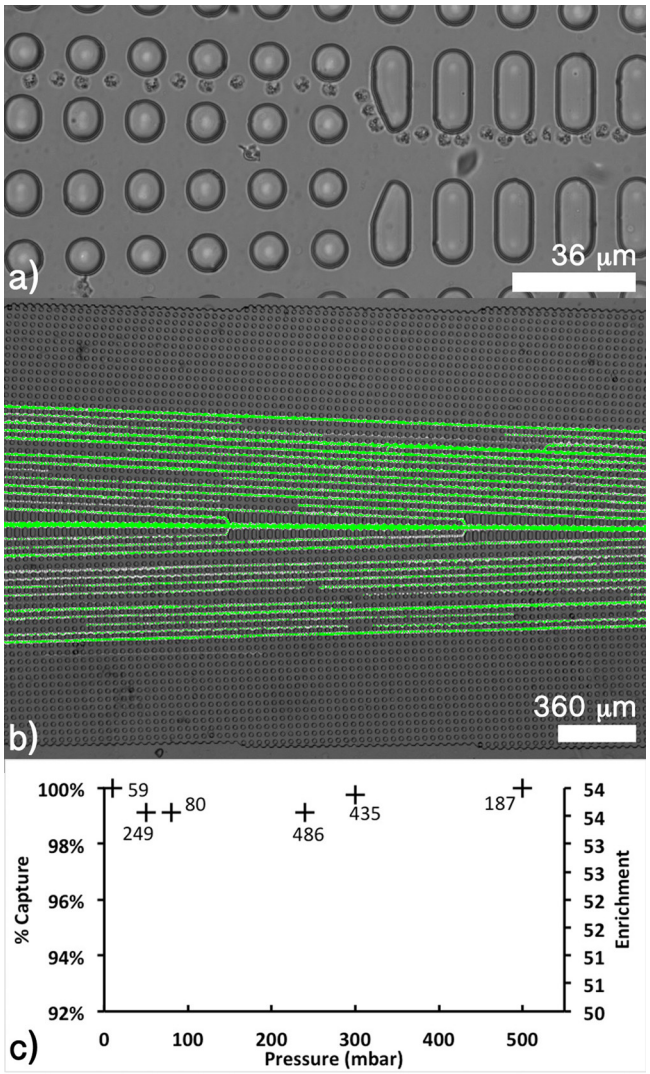

FIG. 5. Performance of cell enrichment: (a) overlaid time-lapse image of a Jurkat cell bumping into the central channel. Flow is left to right; (b) low magnification fluorescence image of SYBR green labelled Jurkat cells in the chip; and (c) percentage of cells in the central channel, and corresponding enrichment at the end of the array versus pressure. Data labels indicate the number of cells in each experiment.

54-fold. The data shown in Figure 3 do not explain why 6 and 7 μm particles fail to concentrate to the -1, 0, and $+1$ exit columns. We hypothesize that the large disturbance to the flow pattern that is centred at g1 negatively affects performance as far away as 10 posts.

In designing our array, we used an analytical model that approximates the relationship between the gap size and fluidic resistance. Using very large posts, small gaps, and very deep etch depths would enable a design that uses a more accurate cube root relationship. It would also be possible to use a more accurate model of channel resistance that allows direct calculation of width, for a given depth and desired hydraulic resistance, such as that developed by Mortensen *et al.*[13] This may result in a higher performance device; however, all of these approaches neglect the pressure dropped when the fluid moves laterally. We suspect that this is significant, particularly around g_1. The experimentally observed flow pattern shows just how much improvement is possible. Full 3D simulations and an automated design process should be capable of producing a geometry with a perfectly constant critical size, i.e., a flat line in Figure 3(a).

Cell enrichment was investigated at different densities, but significant clogging was observed in the central channel at an initial concentration of 3×10^6 cells/ml. These clogs

formed exclusively in the narrowest of central gaps toward the end of the device where cell concentration is the highest. This suggests that cell-cell adhesion is the likely cause. This may be reduced by adding bovine serum albumin to the running buffer.

We did not quantify the off-chip cell concentration and found that adjusting the pressure balance at the two outlets greatly affects the flow ratio. This allows some trade-off between capture efficiency and enrichment. In retrospect, high resistance outlet channels, and less open area between the end of the array and the start of the collection channels, would ensure a more stable ratio of product to waste flow.

V. CONCLUSION

DLD may be considered a mature technology with many users in academia and industry. There have, nevertheless, been significant improvements and developments described in recent years.[14–17] In research-only devices, designers can constrain themselves to flow far away from boundaries by supplying excess buffer in an overly wide device. In every practical device, the designers must concern themselves with flow near the boundaries. This work shows an improvement in boundary treatment, but more significantly, it experimentally maps the flow patterns at those boundaries and shows some crucial shortcomings of our model. In addition, the device presented works nearly flawlessly at concentrating cells by over 50-fold in a single pass, which is just more than a $2\times$ improvement in concentration over prior art.

VI. METHODS

Devices were fabricated using standard SU-8 lithography and PDMS (Polydimethylsiloxane) soft lithography to a depth of $40 \pm 2\,\mu$m. It was essential to use a low UV exposure to achieve post and gap sizes as defined on the photomask. Devices were reversibly bonded to a glass slide containing through holes using the Glass-PDMS-Glass method described in Ref. 18, submerged in a solution containing 2 g/l pluronic F108, and then placed under vacuum (-95 kPa) for at least one hour prior to use. Bead solutions contained 0.1% Tween 20 and 21% glycerol. The glycerol is used to bring the solution density to 1.055 g/ml, near that of the polystyrene spheres.

Jurkat (leukemic T-cell line) cells were cultured in a complete medium (RPMI (Roswell Park Memorial Institute medium) with 10% fetal calf serum and 1000 U/ml penicillin/streptomycin) at concentrations between 1 and 4×10^6 cells/ml. The non-adherent cell mixture was taken from the flask, filtered through a 10 μm nylon mesh strainer, and counted using an automated cell counter. Before imaging, cells were stained with SYBR Green (Thermo Fisher Scientific) as per manufacturers guidelines and then diluted in fresh medium. The micro-device was flushed with approximately 100 μl of AutoMACS running buffer (Miltenyi Biotech) prior to running cells in medium.

Particle trajectories and exit position counts were made using video recorded with a monochrome fluorescence camera and an epi-fluorescent microscope. Images and movies were post-processed and analysed using imageJ. The chip is held in a custom made clamp providing O-ring seals to the backside through-holes and threaded connections to a computer controlled (0–1 bar) pressure regulator (Fluiwell and MFCS by Fluigent).

SUPPLEMENTARY MATERIAL

See supplementary material for plots of fluid flux versus channel gap and fits using a gap-squared and gap-cubed approximation.

ACKNOWLEDGMENTS

We thank A/Professor Linda Bendal (University of Sydney/Westmead Institute for Medical Research) for supplying the cells. This work was supported by the Wireless Medical Devices Research Centre, the Australian Research Council Centre for Nanoscale BioPhotonics, and the Department of Engineering at Macquarie University. Alison Skelley is an employee of GPB Scientific; GPB develops and commercialises microfluidic devices including deterministic lateral displacement technology.

[1]L. R. Huang, E. C. Cox, R. H. Austin, and J. C. Sturm, "Continuous particle separation through deterministic lateral displacement," Science **304**, 987–990 (2004).
[2]D. W. Inglis, J. A. Davis, R. H. Austin, and J. C. Sturm, "Critical particle size for fractionation by deterministic lateral displacement," Lab Chip **6**(5), 655–658 (2006).
[3]J. McGrath, M. Jimenez, and H. Bridle, "Deterministic lateral displacement for particle separation: A review," Lab Chip **14**, 4139–4158 (2014).
[4]M. Yamada and M. Seki, "Hydrodynamic filtration for on-chip particle concentration and classification utilizing microfluidics," Lab Chip **5**(11), 1233–1239 (2005).
[5]D. Di Carlo, R. G. Tompkins, and M. Toner, "Continuous inertial focusing, ordering, and separation of particles in microchannels," Proc. Natl. Aacd. Sci. **104**, 18892–18897 (2007).
[6]M. E. Warkiani, G. Guan, K. B. Luan, W. C. Lee, A. A. S. Bhagat, D. S. Tan, S. C. Lee, W. T. Lim, P. C. Chen, C. T. Lim, and J. Han, "Slanted spiral microfluidics for the ultra-fast, label-free isolation of circulating tumor cells," Lab Chip **14**(1), 128–137 (2014).
[7]M. E. Warkiani, A. Tay, G. Guan, and J. Han, "Membrane-less microfiltration using inertial microfluidics," Sci. Rep. **5**, 11018 (2015).
[8]D. W. Inglis and N. Herman, "A scalable approach for high throughput branch flow filtration," Lab Chip **13**(9), 1724–1731 (2013).
[9]S. C. Gifford, A. M. Spillane, S. M. Vignes, and S. S. Shevkoplyas, "Controlled incremental filtration: a simplified approach to design and fabrication of high-throughput microfluidic devices for selective enrichment of particles," Lab Chip **14**(23), 4496–4505 (2014).
[10]H. Xia, B. C. Strachan, S. C. Gifford, and S. S. Shevkoplyas, "A high-throughput microfluidic approach for 1000-fold leukocyte reduction of platelet-rich plasma," Sci. Rep. **6**, 35943 (2016).
[11]D. W. Inglis, M. Lord, and R. E. Nordon, "Scaling deterministic lateral displacement arrays for high throughput and dilution-free enrichment of leukocytes," J. Micromech. Microeng. **21**, 054024 (2011).
[12]D. W. Inglis, "Efficient microfluidic particle separation arrays," Appl. Phys. Lett. **94**, 013510 (2009).
[13]N. A. Mortensen, F. Okkels, and H. Bruus, "Reexamination of Hagen–Poiseuille flow: Shape-dependence of the hydraulic resistance in microchannels," Phys. Rev. E **71**, 057301 (2005).
[14]K. K. Zeming, S. Ranjan, and Y. Zhang, "Rotational separation of non-spherical bioparticles using I-shaped pillar arrays in a microfluidic device," Nat. Commun. **4**, 1625 (2013).
[15]K. K. Zeming, T. Salafi, C. H. Chen, and Y. Zhang, "Asymmetrical deterministic lateral displacement gaps for dual functions of enhanced separation and throughput of red blood cells," Sci. Rep. **6**, 22934 (2016).
[16]S. H. Holm, J. P. Beech, M. P. Barret, and J. O. Tegenfeldt, "Simplifying microfluidic separation devices towards field-detection of blood parasites," Anal. Methods **8**(16), 3291–3300 (2016).
[17]E. Henry, S. H. Holm, Z. Zhang, J. P. Beech, J. O. Tegenfeldt, D. A. Fedesov, and G. Gompper, "Sorting cells by their dynamical properties," Sci. Rep. **6**, 34375 (2016).
[18]D. W. Inglis, "A method for reducing pressure-induced deformation in silicone microfluidics," Biomicrofluidics **4**(2), 026504 (2010).